Effect of coupling excess pore pressure and soil deformation on nonlinear SSI in liquefiable soil deposits

Silvana Montoya Noguera, Fernando Lopez-Caballero

Effect of coupling excess pore pressure and soil deformation on nonlinear SSI in liquefiable soil deposits

S. Montoya-Noguera[1,2] and F. Lopez-Caballero[1]
[1]Laboratory MSSMat CNRS UMR 8579, CentraleSupélec, Paris-Saclay University, Châtenay-Malabry 92290, France
[2]Present institution: Department of Architecture and Civil Engineering, City University of Hong Kong, Tat Chee Avenue, Kowloon, Hong Kong

Abstract
The current seismic design philosophy is based on nonlinear behavior of structures where the foundation soil is often simplified by a modification of the input acceleration depending on the expected site effects. The latter are generally limited to depend on the shear-wave velocity profile or a classification of the site. Findings presented in this work illustrate the importance of accounting for both soil nonlinearity due to seismic liquefaction and for soil-structure interaction when dealing with liquefiable soil deposits.
This paper concerns the assessment of the effect of excess pore pressure (Δp_w) and deformation for the nonlinear response of liquefiable soils on the structure's performance. For this purpose a coupled Δp_w and soil deformation (CPD) analysis is used to represent the soil behavior. A mechanical-equivalent fully drained decoupled (DPD) analysis is also performed. The differences between the analyses on different engineering demand parameters are evaluated. The results allow to identify and to quantify the differences between the analyses. Thus, it is possible to establish the situations for which the fully drained analysis might tend to overestimate or underestimate the structure's demand.

Keywords: Seismic liquefaction ; Effective stress analysis ; Soil-structure interaction ; Nonlinearity

1 INTRODUCTION

Sufficient evidence has been identified to proof the importance of site effects on the surface ground motion. Still, in the earthquake engineering practice, the effects of nonlinear soil behavior on the dynamic soil-structure interaction (SSI) are either neglected or simplified. Moreover, when these effects are taken into account, in most cases the nonlinear soil response is modeled with fully drained analysis that do not account for the excess pore pressure (Δp_w) generation which controls the behavior of liquefiable soils. In contrast, coupled analysis allows the modeling of the generation, redistribution and eventual dissipation of Δp_w during and after earthquake shaking. While small or no volume change associated with shear strain is presented, use of fully drained analysis may be justified. For typical liquefiable soils at relatively shallow depths, a threshold shear strain below which no Δp_w will develop has been identified at about 10^{-4} (Drenevich and Richart 1970; Dobry and Swiger 1979; Dobry et al. 1982). Above this threshold effective mean stress changes which will affect the material properties. In such situations, coupled effective stress analysis seem more appropriate (Yoshida and Iai 1998).

Recent studies, performed by Hartvigsen (2007), Yoshida (2013) and Montoya-Nougera and Lopez-Caballero (2016) have evaluated the effects of coupling Δp_w and deformation on the soil behavior. In these studies, focus was given mainly to the effects on the ground motion amplitude and frequency content. A summary of this research is briefly presented in the

following section. Concerning peak ground acceleration (PGA), all studies agree that accounting for Δp_w will in general incur in lower values; thus without it the results will be conservative. However, regarding the response spectra of acceleration (PSA), higher values could be presented for long periods; which will be prejudicial for flexible buildings. All of these analyses have been performed in free-field 1D conditions and these effects have not been analyzed on the performance of structures founded on cohesionless soils.

The aim of this work is to assess the effects of Δp_w generation on the performance of a structure founded on liquefiable soil. For this purpose a nonlinear 2D soil-structure interaction (SSI) model is analyzed under a wide range of unscaled earthquake signals. Two structures with different predominant periods are used in order to account for different cases of SSI. In the interest of quantifying the effects, two mechanically-equivalent models -one with coupled Δp_w and soil deformation (CPD) and one fully drained (DPD) - were performed with the same effective-stress analysis. Three aspects were evaluated on the structure: i) the response spectra of acceleration , ii) the relative settlement and iii) the inter-story drift.

1.1 Summary of previous findings

In this work, the comparison is made between analyses with and without Δp_w in the interest of evaluating solely the effect of coupling Δp_w and deformation. To address this subject, only a limited number of studies have been published. Each study used a different technique but in all, the fundamental variation is in the presence or lack of Δp_w. For clarity the two analyses will be referred to as CPD and DPD.

Hartvigsen (2007) performed a series of CPD and DPD analyses of 1D wave propagation in different soil columns and subjected to a variety of earthquake motions. The main conclusions of the parametric study were also published by Kramer et al. (2011). In total, nine 20-m thick soil profiles with varying depths of liquefiable soil were subjected to 139 input motions. The model used is written in effective stresses but for the DPD analysis, the bulk modulus of the pore fluid was reduced to a very low value. Thus, while the weight of the water contributes to the dynamic soil response (i.e. the inertial effect), there is no generation of Δp_w. As a result, they presented a correction function for the surface PSA obtained by the ratio of CPD and DPD analyses. This correction, called the response spectra ratio ($RSR = PSA^{CPD}/PSA^{DPD}$), is a function of period and of the loading parameter (L) that is the inverse of the factor of safety (FS) defined by the cyclic stress approach (Seed and Idriss 1971). RSR can then be applied to the PSA values obtained with a total stress analysis to obtain a more accurate response spectrum for liquefiable soils. Among the main features of this factor is that even for very high FS, an amplification is evidenced -i.e. RSR > 1 - above a certain period that increases as FS decreases. Interestingly, as FS decreases a peak of amplification and of deamplification evolves. The combination of the mid-period deamplification trough and long period amplification evidences the shift to low frequencies that occurs as a result of soft-site amplification (Beresnev and Wen 1996). For the lowest liquefaction resistance shown (FS=0.5), maximum RSR is approximately 1.3 at T≈10s and the minimum is 0.3 at T≈0.5s. A regression analysis was used to obtain RSR but the correlation between the residuals was low, hence the applicability of the function is unlikely. Additionally, the use of a loading parameter reduces the analysis to a simplified procedure where the input motion variability is only expressed by PGA and the magnitude scaling factor while the soil response is only described by the SPT blow count and the reduction factor.

Similarly, Yoshida (2013) compared the CPD and DPD analyses. A total of 268 sites were subjected to 11 earthquake motions. Again the only difference between the analyses is the

consideration of excess pore water pressure generation or not; however, no information on how this was performed was stated. The comparison was focused on five frequently used intensity measures of the surface time history: the peak acceleration (PGA), peak velocity (PGV), peak displacement (PGD), instrumental seismic intensity (I_{JMA}) and spectral intensity (SI). The PGA results from the CPD analysis were consistently smaller than the ones obtained by the DPD one. Whereas for PGD, the CPD results were greater, which could affect the design of underground structures such as piles and pipelines. The differences between the analyses were smaller for the other intensity measures. Again, the program used for these analyses only took into account the SPT blow count to describe the soil behavior. In contrast with Hartvigsen results, no clear trend between the two analyses was identified, possibly due to the great variability of sites tested, some of those with no liquefiable soil.

Gingery et al. (2014) followed a similar procedure as that of Hartvigsen (2007) but applied to ground motion prediction equations (GMPEs) that do not account for liquefaction. The four GMPEs used were the updated attenuation relationships for the western U.S. from the Next Generation Attenuation (NGA) project (Chiou et al. 2008) that accounted for soil conditions. An amplification function (AF) for each GMPE was calculated from the logarithmic ratio of PSA of recorded motions in 19 liquefiable soil deposits and the evaluated NGA GMPE, i.e. $\ln(AF) = \ln(PSA^{\text{rec}}/PSA^{\text{NGA}})$. The correction functions presented in general a similar trend as the RSR proposed by Hartvigsen (2007) but with higher maximums and minimums; although these factors are hard to compare, as they are applied to different analyses (i.e. CPD vs DPD and measured vs. GMPEs). However, an interesting aspect of these results is that added to the known long period amplification, a second amplification was observed for short periods (around T≤0.05 seconds) which could be the result of acceleration spikes that occur in association with the dilatational part of liquefaction phase transformation behavior.

Finally, the work presented by Montoya-Noguera and Lopez-Caballero (2016) also analyzed the effect of coupling Δp_w and soil deformation on 1D wave propagation. Besides evaluating PSA and other intensity measures at the surface; a detailed analyses of time evolution and maximum profiles was also presented. Concerning PSA, the CPD results present an amplification in long periods and also at periods around 0.05s, as evidenced by Hartvigsen (2007). The differences between CPD and DPD response spectra increase with the amount of liquefied soil in the deposit. One interesting finding was that although for most motions tested PGA is greater for the DPD analysis, some cases present lower values, even down to 40% smaller. In contrast, for the Arias intensity of surface acceleration and the co-seismic settlement, DPD values were up to six times greater than CPD ones. Regarding the soil profile, clear relations were found between acceleration, shear strain and liquefaction ratio for the CPD analysis; however, shear strains evolution with depth do not relate with acceleration in the DPD analysis. It should be mentioned that this paper was the first phase of a larger study and that the present work is the scale up to a 2D more complex model. To the best knowledge of authors, no study has been published that accounts for the effects of coupling Δp_w and soil deformation on SSI. While PGA and other intensity measures can be lower with CPD analysis in 1D soil profiles, the added effect of the 2D pore pressure's migration and distribution, and of the structure's load and seismic performance, it could be prejudicial for the analysis.

2 NUMERICAL MODEL

Two soil-structure models are considered in this work. They consist of reinforced concrete (RC) buildings with a shallow rigid foundation, standing on saturated cohesionless soil. A schema of the models is shown in Figure 1. One structure is modeled as an RC frame of one

span and two stories and the other is a single-degree-of-freedom (SDOF). The dynamic performance of the structures is different as they have different height, weight and predominant periods. Both structures lay on a 6m rigid foundation. All structural elements are elasto-plastic. Concerning the soil model, a 50m wide and 20m thick deposit of loose-to-medium (LMS) sand is overlaying an elastic bedrock. The shear modulus increases with depth and the equivalent shear wave velocity of the first 20m ($V_{s\,20}$) is 200 m/s. The fundamental elastic frequency (f_0) of the soil profile, calculated with a low-strain frequency analysis, is equal to 2.63Hz. An elastoplastic multi-mechanism model is used to represent the soil behavior. Under the deposit, an engineering bedrock representing a half-space medium is modeled with an isotropic linear elastic behavior and a shear wave velocity (V_s) equal to 550m/s. The ground water table is located 1m below the surface.

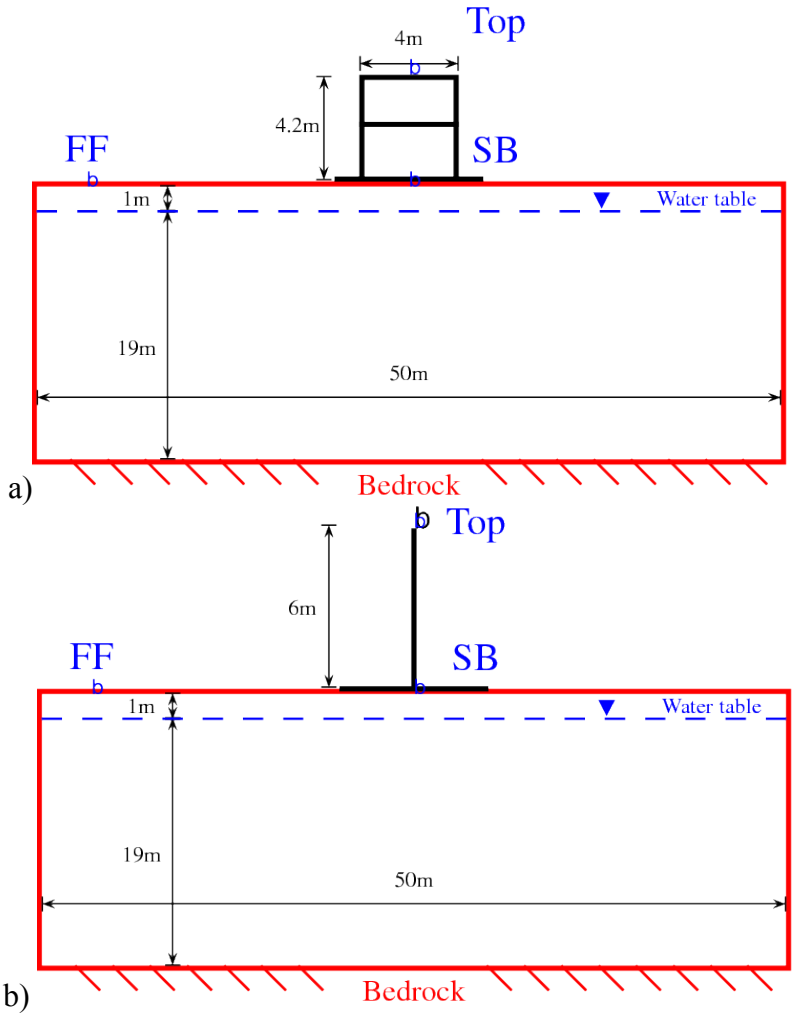

Figure 1: Schema of the numerical model for a) B01 and b) T040

2.1 Finite element model

As the soil is assumed to be horizontally homogeneous, a 2D finite element computation was performed. The general purpose finite element code GEFDyn (Aubry and Modaressi 1996) was used. The saturated soil was modeled using quadrilateral isoparametric elements with eight nodes for both solid displacements and fluid pressures. The soil model is 20m depth, 50m wide. The size of the elements is 0.5x0.5m^2, which is in agreement with the suggestions made by Foerster and Modaressi (2007) to prevent numerical dispersion even for strong motion excitations. For a maximum frequency of 15Hz (of engineering interest in this study) and a minimum initial V_s of 135m/s (at the surface), a minimum of 36 points per wavelength

is allowed in the elastic domain. The number of points is high, although it will decrease as the soil softens and the V_s decreases. For the time discretization in the dynamic analysis, an implicit Newmark numerical integration scheme is used with parameters $\gamma_N = 0.611$ and $\beta_N = 0.301$. This induces a minimal numerical damping that affects principally the elastic response of the model, but allows an optimal high-frequency dissipation with minimal low-frequency impact (Hughes, 2000; Montoya-Noguera and Lopez-Caballero 2016). To take into account the interaction effects between the structure and the soil, a modified width plain-strain condition was asumed in the model. This approach was developed and verified with 3D models by Saez et al. (2013). In this case an out-of-plane dimension of 4m is used for the soil profile.

2.1.1 Coupled and Decoupled dynamic approach

A coupled dynamic approach derived from the $\boldsymbol{u} - p_w$ formulation of the Biot's generalized consolidation theory (Zienkiewicz and Shiomi 1984; Zienkiewicz and Taylor 1991) was introduced in the code by Modaressi (1987). This formulation consists of neglecting fluid acceleration terms and its convective terms so that the unknown variables remain the displacement of the solid $\boldsymbol{u}$ and the pore water pressure p_w. As further simplifications, soil grain compressibility is assumed to be null and thermal effects are ignored. The behavior of the solid skeleton is derived assuming the principle of effective stress as proposed by Terzaghi (1943), where the total stress tensor ($\boldsymbol{\sigma}$) is separated into two components: the effective stress tensor ($\boldsymbol{\sigma}'$) and the pore pressure (p_w). Which reads: $\boldsymbol{\sigma} = \boldsymbol{\sigma}' - p_w \boldsymbol{I}$ with $\boldsymbol{I}$ the identity second order tensor. Under such hypotheses the set of governing equations is:

- Overall equilibrium for the soil-fluid mixture

$$\mathrm{div}\boldsymbol{\sigma}' - \mathrm{grad}(p_w) + \rho \boldsymbol{g} = \rho \ddot{\boldsymbol{u}} \qquad (1)$$

where ρ is the total average unit mass ($\rho = n\rho_w + (1-n)\rho_s$); n is the soil porosity; ρ_w, the fluid mass; ρ_s, the soil particle mass; $\boldsymbol{g}$, the gravity acceleration vector and $\boldsymbol{u}$, the solid skeleton displacement.

- Equilibrium of water and flow conservation equation using generalized Darcy's law. Assuming each phase as homogeneous:

$$\mathrm{div}\dot{\boldsymbol{u}} - \mathrm{div}(\boldsymbol{K}(\mathrm{grad}(p_w) - \rho_w \boldsymbol{g})) - \mathrm{div}(\boldsymbol{K}\rho_w \ddot{\boldsymbol{u}}) + \frac{\dot{p_w}}{Q} = 0 \quad (2)$$

where $\boldsymbol{K}$ is the permeability tensor defined by $\boldsymbol{K} = \boldsymbol{\kappa}/\rho_w \boldsymbol{g}$, $\boldsymbol{\kappa}$ being the kinematic permeability tensor, and Q is the compressibility parameter ($Q^{-1} = n/K_w + (1-n)/K_s$), K_w and K_s being the fluid and solid compressibility, respectively.

Note that the pore water pressure generation and dissipation will depend on the permeability tensor and the compressibility parameter. Hence, the DPD analysis can be done by either reducing the compressibility to nearly zero as was done by Hartvigsen (2007), or by increasing the permeability to infinity. In this study another approach was chosen. It consists in keeping the same inertial effects, while no excess pore pressure is generated. For the inertial effects, the DPD analysis has a total unit mass equal to the coupled model, so the weight of the water contributes to the dynamic soil response (equation 1). Thus, in the DPD analysis the pore water pressures are computed based on a fixed water table level. It is worth noting that both CPD and DPD are performed with effective-stress analysis and with the same constitutive model.

2.1.2 Boundary conditions

Concerning boundary conditions, as the signal propagation is one-dimensional and as the response of an infinite semi-space is modeled, equivalent boundaries have been imposed on the lateral nodes (i.e. the normal stress on these boundaries remains constant and the displacements of nodes at the same depth in two opposite sides are the same in all directions) (Lopez-Caballero and Modaressi 2011). As the lateral limits of the problem are considered to be far enough from the structure in the middle of the model, periodic conditions are verified. For the bedrock's boundary condition, paraxial elements simulating "deformable unbounded elastic bedrock" have been used (Modaressi and Benzenati 1994). The paraxial elements efficiently evacuate outgoing (diffracting) waves in a local domain. While the vertically incident shear waves, defined at the outcropping bedrock, are introduced into the base of the model after deconvolution. Thus, the obtained movement at the bedrock is composed of both incident and reflected waves.

For the CPD analysis, during the dynamic loading, p_w are allowed to change below the groundwater table as a result of soil contraction and dilation due to shear strains. For the bedrock's boundary, the pore pressure conditions are assumed to be impervious. Therefore, no flux occurs across the interface boundary between the studied domain and the underlying semi-infinite space.

2.2 Soil Model

The soil deposit of cohesionless sand presents a maximum shear modulus (G_{max}) profile dependent on the mean effective stress (p'), as follows:

$$G_{max} = G_{ref}\left(\frac{p'}{p'_{ref}}\right)^{n_e} \quad (3)$$

where G_{ref} is the shear modulus at the reference stress (p'_{ref}) and n_e is the degree of nonlinearity. In this case, G_{ref} equals to 290MPa , p'_{ref} to 1MPa and n_e to 0.5. Thus, at free field G_{max} increases with depth as shown in Figure 2. The ground water table is placed 1m below the surface and for this superficial layer, G_{max} is constant (i.e. n_e= 0). The engineering bedrock is assumed to be deformable. It has an isotropic linear elastic behavior with a shear-wave velocity (V_s) equal to 1700m/s and a shear modulus (G) of 5.8 GPa. The impedance ratio between the bedrock and the deposit (I) is 7.8, evaluated as $I = (V_s^r \boldsymbol{\rho}^{\mathbf{r}})/(V_s^s \boldsymbol{\rho}^{\mathbf{s}})$, where superscripts r and s denote bedrock and bottom of the soil deposit. This value is sufficiently large to assume an elastic behavior of the engineering bedrock compared to the soil deposit.

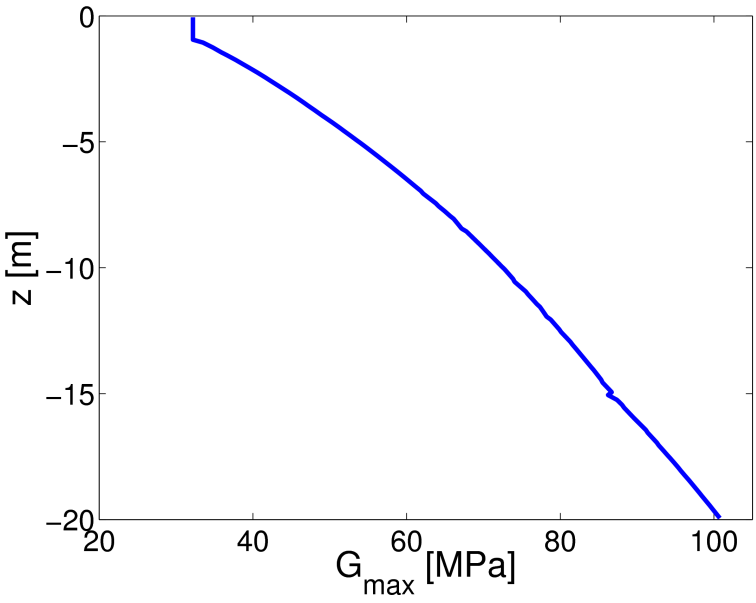

Figure 2: Initial shear modulus profile at free-field

2.2.1 Soil constitutive model

The elastoplastic multi-mechanism model used was developed at CentraleSupélec, formerly called École Centrale Paris (ECP), in the early 80s (Aubry et al. 1985; Modaressi 1987) and has been improved thereafter. The family of ECP models has been validated in a number of studies to simulate different kinds of loadings: seismic soil response of vertical arrays (Foerster and Modaressi 2007b; Regnier et al. 2015b), seismic response of soil structures (Sica et al. 2008) and pile installation (Berenguer 2014) among others.

The model uses a Coulomb type failure criterion and follows the critical-state concept. It can take into account a large range of deformations due to the decomposition into three domains (pseudo-elastic, hysteretic and mobilized) and the evolution of hardening based on the plastic strain. To model the cyclic behavior it uses a kinematic hardening which relies on the state variables at the last load reversal. For a complete description of the model refer to Aubry et al. (1982), Hujeux (1985), and Lopez-Caballero and Modaressi-Farahmand-Razavi (2010) among others. The soil model parameters were determined with the procedure defined by Lopez-Caballero et al. (2007) and are found in Montoya-Noguera and Lopez-Caballero (2016).

2.3 Structural model

Two models were used in order to analyze the effect of the coupling Δp_w and soil deformation for different predominant periods. The structures used will be called B01 and T040 and are reinforced concrete buildings with different size, weight and stiffness. In order to simulate the B01 structure, plastic hinge beam-column elements are used which take into account axial force (P) and bending moment (M) interaction (Prakash et al. 1993). This structure is a large-scale, one-span, two-story frame model proposed by Vechio and Emara (1992). In contrast, the T040 is a single-degree-of-freedom (SDOF) modeled with an elastic perfectly plastic behavior and is equivalent to a one-span, three-story building (Saez et al. 2013). It is a simplified model of a moment frame mid-rise structure according to the building type classification of HAZUS-MH MR3 (2003). This additional structure is used in this study to highlight the effects of the soil behavior in the structure performance near resonance. The main characteristics of both structures are shown in Table 1.

Property	B01	T040
Total height [m]	4.2	6
Width [m]	4	N/A
Mass [ton]	45	120
Fundamental fixed-base period T_0 [s]	0.24	0.40

Table 1: Structures' properties

The structure foundation is modeled as a rigid block of 10cm thick and 6m wide. Between the foundation and the soil, interface elements are used to allow relative movement of the structure with respect to the soil, in order to avoid the traction effect. These elements follow a Coulomb-type plastic criterion.

The building's weight affects the stress state (horizontal, vertical and shear) and also the volumetric deformations, hence it affects the maximum shear modulus (G_{max}) defined previously by equation (3). Thus, the effect of the structure's inertial load on the soil behavior is seen on the differences in G_{max} along the horizontal axis which is shown in Figure 3 for both structures. Note how the soil under the building presents higher values compared to free-field for shallow depths until around 6m but for deeper soil, the G_{max} values are decreased. Additionally, because T040 is heavier, this increase and decrease are greater and affect lower depths. As the coefficient of earth pressure at rest (k_0) also increases with the building load, the surrounding soil is stiffened but without the effect of the shear stress. Thus, a slight increase in $G_{max}$is visible in the soil on this region, specially visible below 10m in T040 model (Figure 3b). It is worth noting that areas where the G_{max} increased might present higher liquefaction resistance.

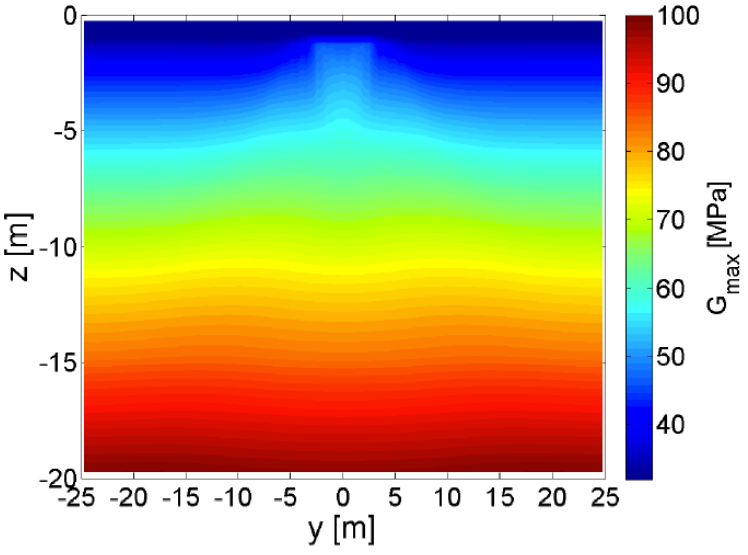

a)

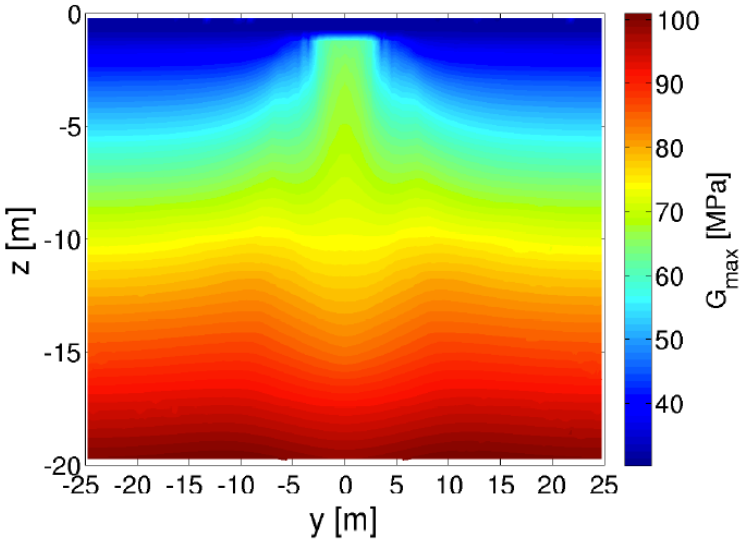

b)

Figure 3: Shear modulus G_{max} distribution in the deposit before shaking for a) B01 and b) T040

Concerning the initial seismic behavior, a scaled motion with a very low amplitude (i.e. PHA$\approx 10^{-5}g$) was used to evaluate the pseudo-elastic behavior of both soil and structure. Figure 4 shows the transfer functions ($|TF|$) - with fixed base and with soil-structure interaction (SSI) effects (top/FF) for the two structures. In addition, $|TF|$ of the soil deposit (FF/bedrock) is also shown. Firstly, it is interesting to note that, even if B01 has two stories, only one resonant frequency (f_{str}^{FB}) is observed - as the other one is above 15Hz. Hence both structures behave as SDOFs. The SSI effects consist of a shift to lower frequencies due to the flexibility of the foundation soil and a deamplification due to the material and radiation damping added by the soil (Mylonakis and Gazetas 2000). As expected, structure B01 being more rigid presents a higher interaction with the soil foundation; hence, the deamplification and the frequency shift are greater. Hence, the relative position of the fundamental frequency of the soil with respect to that of the structure and the frequency content of the input motion is very important for the inelastic dynamic SSI effects (Saez et al. 2013). Thus, as T040 main frequency is lower than that of the soil, higher SSI effects are expected when nonlinear soil degradation causes a shift of the soil frequency to lower values.

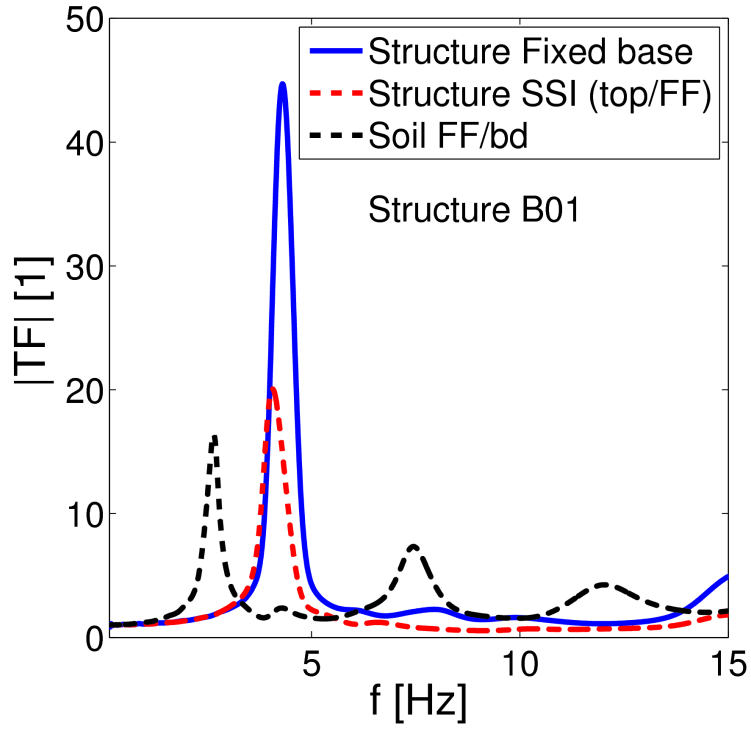

a)

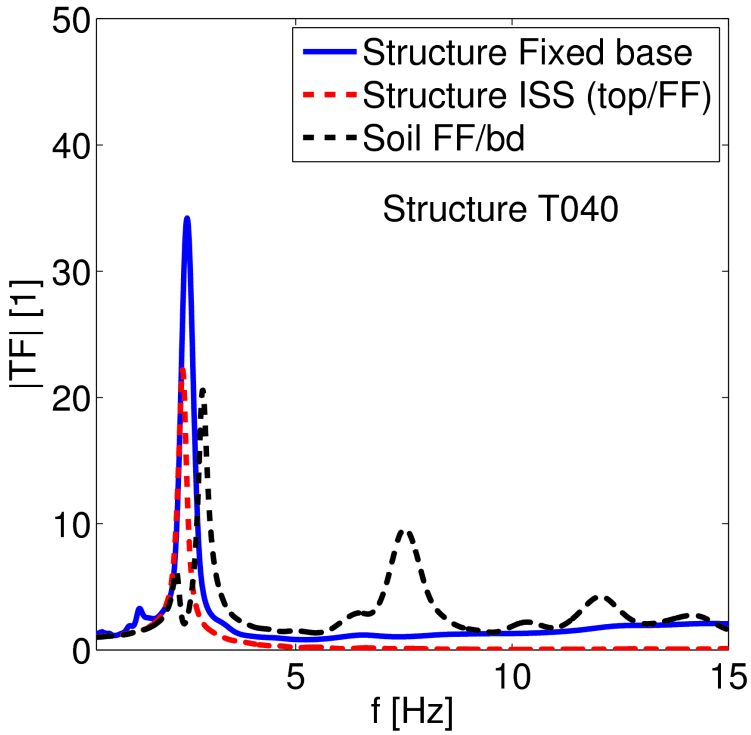

b)

Figure 4: Transfer function of the free-field and the structure for a) B01 and b) T040

2.4 Input earthquake motions

Ninety unscaled records were chosen from the Pacific Earthquake Engineering Research Center (PEER) database. The signals used were recorded near the source - with a site-to-source distance below 70km- and in dense soil conditions - i.e. 30m averaged shear-wave velocity ($V_{s\,30}$) above 600m/s. These signals are supposed to have minimal noise and are appropriate for an outcropping bedrock condition. The events range between 6.2 and 7.7 in moment magnitude.

The statistics of some earthquake parameters calculated at outcropping conditions are shown in Table 2. These intensity measures are peak horizontal acceleration (PHA), peak ground velocity (PGV), mean period (T_m), predominant period (T_p), period of equivalent harmonic wave ($T_{V/A}$), Arias intensity (I_A), significant duration (D_{5-95}), root-mean-square intensity (I_{RMS}), spectral intensity (SI) and specific energy density (SED). The coefficient of variation (CV) is high for all parameters and it is about 130% for I_A. A high variation in I_A is of great importance given that after the sensitivity analysis performed by Lopez-Caballero and Modaressi-Farahmand-Razavi (2010), it was proved to be the most influential input variable on the average liquefaction developed on the upper 10m of the deposit, known as $Q_{H=10m}$. Figure 5 shows the response spectra of all the input earthquake motions; accelerations were filtered to 20Hz and the spectral amplitude has a 5% structural damping. Similarly, a great variation is presented on the response spectra.

Table 2: Earthquake characteristics

Parameter	Range	Mean	CV [%]	Median
PHA [g]	0.03 – 1.16	0.34	85	0.26
PGV [cm/s]	3.15 – 121	30.52	92	21.80
T_m [s]	0.22 – 0.87	0.49	31	0.47
T_p [s]	0.09 – 0.65	0.30	51	0.25
$T_{V/A}$ [s]	0.21 – 0.85	0.48	35	0.48
I_A [m/s]	0.02 – 11.8	2.17	136	0.64
D_{5-95} [s]	4.12 – 36.47	17.04	58	14.59
I_{RMS} [m/s^2]	0.04 – 1.48	0.46	79	0.41
SI [m]	0.04 – 1.16	0.37	80	0.30
SED [cm^2/s]	28.7 – 34098	2705	241	499

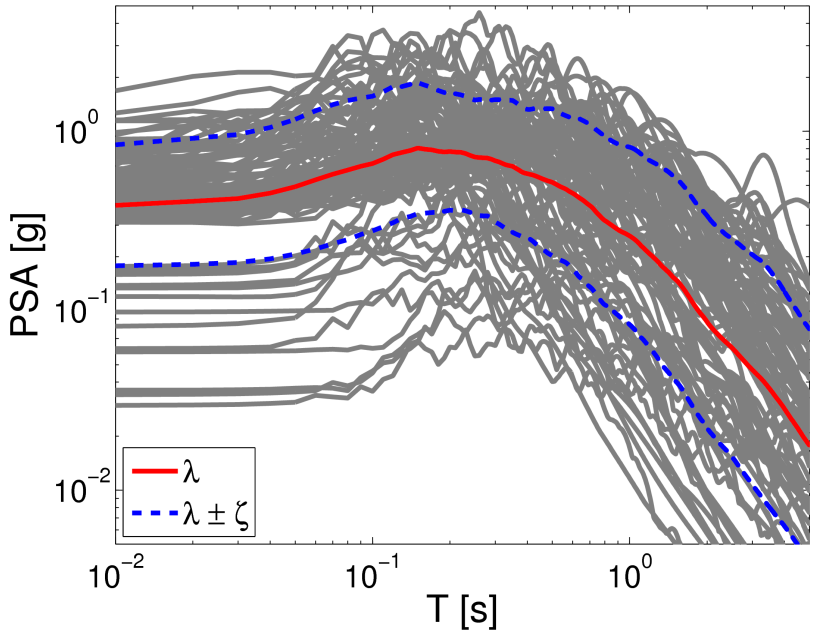

Figure 5: Response spectra of acceleration for the outcropping motions. The geometric mean (λ) and standard deviation (ζ) are shown in red and blue, respectively.

3 ANALYSIS AND RESULTS

The effect of coupling Δp_w and soil deformations on a soil-structure model is highly complex and will affect several aspects of the response. First the analysis for one input motion will be shown and then some results concerning all the motions will be addressed.

As recalled before, Montoya-Noguera and Lopez-Caballero (2016) have already analyzed the effects of such coupling on the nonlinear seismic soil response. In that study, a 1D model of the same soil deposit was used and compared to a denser soil deposit. As differences in the response are given by the liquefaction apparition and the pore pressure generation, in this study, only the more liquefiable soil is used for the SSI model.

As explained in section 2.1.1, the main difference in the analyses will be given by the strains due to pore pressure generation. As the latter increases, the difference in the soil deposit in terms of acceleration, shear strain and settlement increases. Figure 6 and Figure 7 show the time histories of these parameters for one motion tested.

First, in Figure 6 the evolution of the liquefaction ratio ($r_u = \Delta p_w / \sigma_0'$) is shown for a profile far from the structure -i.e. in free field. In this analysis, liquefaction is described as the significant reduction of the effective stress and therefore accounts for both phenomena: *true liquefaction* (when $r_u = 1.0$) and *cyclic mobility* (i.e. $0.8 < r_u < 1.0$ with development of large strains) (Koutsourelakis et al. 2002; Popescu et al. 2006). Thus, liquefaction is said to be triggered when r_u equals 0.8. The location of liquefaction is dependent on the frequency content and the soil stiffness evolution. In general, high frecuency accelerations tend to liquefy shallow soil while low frequency ones tend to liquefy deeper soil (Popescu, 2002; Lopez-Caballero and Modaressi-Farahmand-Razavi, 2008). Real motions have complex frequency content that varies in time thus liquefaction can be triggered at different locations. For the case shown in Figure 6, liquefaction is first triggered at shallow soil as initially the motion contains primarily high frequency amplitudes, and then liquefaction appears in deeper soil when the motion contains low frequency content. The pore pressure generation and dissipation through depth evolves as the motion's frequency content aswell as the soil stiffness changes. The frequency content of the motion is modified due to pore-pressure generation as has been shown in previous studies (Kramer et al., 2015; Montoya-Noguera and Lopez-Caballero, 2016). Additionally, the soil stiffness is reduced in zones where liquefaction is triggered first and pore-pressure might migrate to deeper aswell as shallower depths. It can be noted that although the same soil properties are used throughout the deposit, due to the increase in mean stress and the stress ratio difference, pore pressure generation does not increase simultaneously through depth. Additionally, the time evolution of the frequency content of the motion causes liquefaction at different depths in different instants. For this motion, liquefaction first appears between 6 and 7m depth at around 8s, then it starts in two other deeper zones. After the predominant duration of the motion, i.e. at around 15s, the pore pressure migrates to other depths. At the end of shaking, r_u is almost evenly distributed and it is still above 0.8 for depths between 5 and 15m.

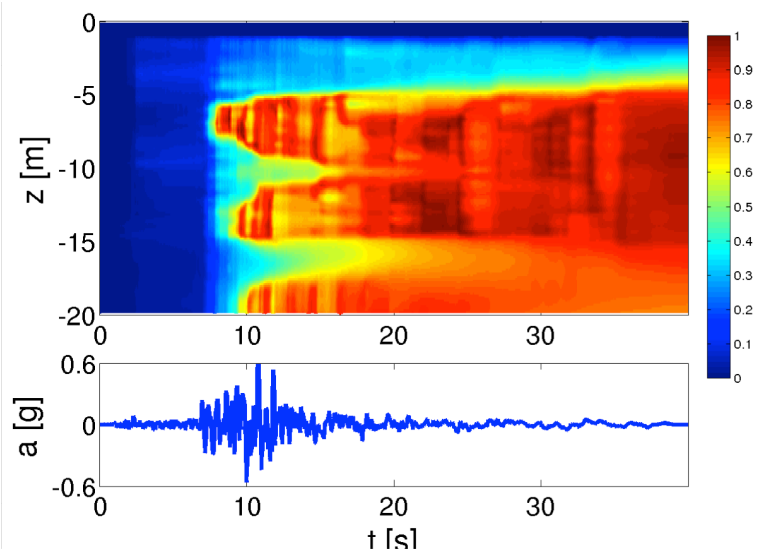

Figure 6: Time history liquefaction ratio at free field for one motion tested. The outcropping acceleration time history is shown below.

The time history of the acceleration at the structure's base is shown in Figure 7 for both analyses. With respect to the outcropping motion shown in the previous figure, the peak amplitude is almost one third for the DPD model and is slightly lower for the CPD one. The differences in time between the analyses is easily related to the liquefaction evolution with time also shown previously. After the first liquefaction triggering at 8s, the responses start to differ. The CPD model presents a shift towards low frequencies after approximately 10s, while the DPD shows higher spikes at higher frequencies. Similarly, the relative settlement of the structure with respect to free field ($|u_z|$), shown in Figure 7, evolves differently starting from 8s. Due to the pore pressure migration, evidenced in Figure 6, differences in $|u_z|$ are greater after the predominant duration of the motion and by the end of the shaking, the CPD model presents results more than 4 times higher than the DPD.

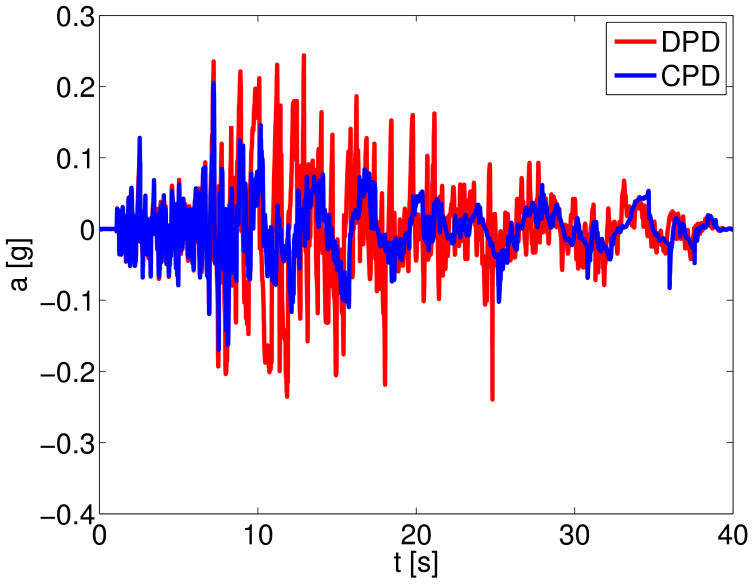

a)

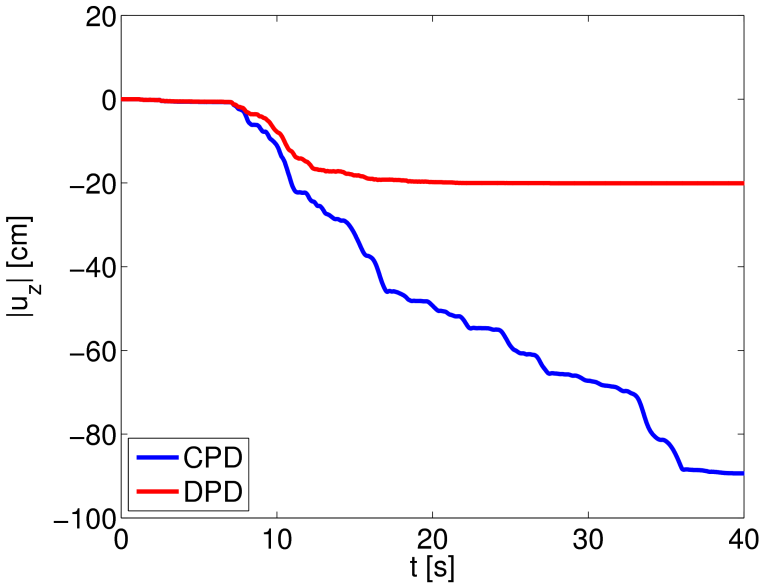

b)

Figure 7: Time history analysis for one motion tested: a) Surface acceleration at structure's base and b) relative settlement of the structure with respect to free field

Concerning the entire deposit an important issue is the building load and the effects on the soil behavior. Figure 8 shows the liquefaction ratio at the end of shaking and the maximum shear strain for all the deposit. As the soil under the structure is stiffened, liquefaction is not presented there; however, around this area and because of the differences in the stress state, high r_u values appear beyond the structure's influence. On that account, the maximum shear strains are higher for the CPD model; often twice the value of the DPD one. Furthermore, while for the CPD model, the maximum values appear to be related to the places where maximum r_u values are located; for DPD, the maximum values are more evenly distributed through the deposit.

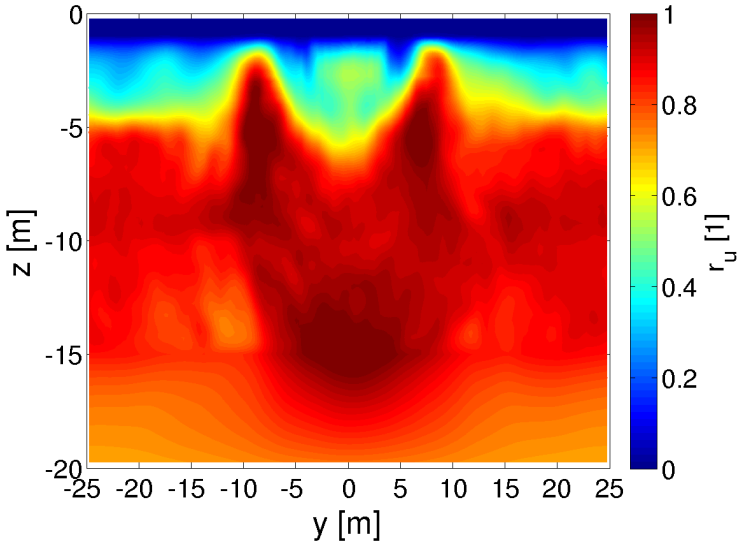

a)

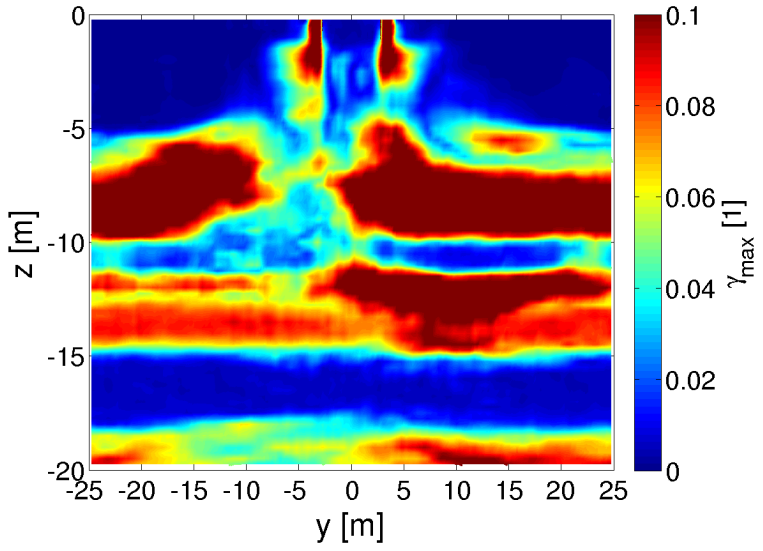

b)

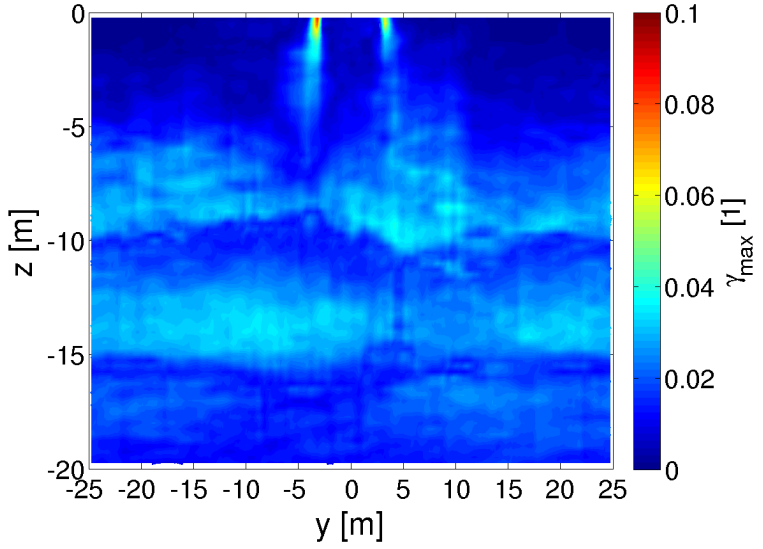

c)

Figure 8: Soil deposit analysis for one motion tested: a) Liquefaction ratio at the end of shaking and maximum shear strain for b) CPD and c) DPD models.

In terms of time history and in the entire deposit, the response for each motion varies greatly, due to the differences in frequency, energy and duration content of the motion. Hence to analyze all the motions tested, focus will be given to three engineering demand parameters: (1) peak ground acceleration (PGA) at the structure's base, (2) co-seismic relative settlement of the structure with respect to free field ($|u_z|$) and (3) maximum inter-story drift (ISD). These parameters are often used for seismic structure performance when SSI effects are taken into account and are often used for numerical analysis.

To relate the differences between the CPD and DPD analyses with the level of liquefaction, results are ranged by the liquefaction index ($Q_{H\cdot L}$). This parameter was firstly introduced in 1D by Shinozuka and Ohtomo (1989) and it is extended to a 2D model as:

$$Q_{H\cdot L} = \frac{1}{H\cdot L}\int_0^H \int_0^L r_{u,\,\mathrm{end}}(y,z)\mathrm{d}y\mathrm{d}z \qquad (4)$$

where $r_{u,\,\mathrm{end}}$ is the liquefaction ratio, previously defined, evaluated at the end of shaking.

When $Q_{H\cdot L}$ is equal to unity, it means that liquefaction is present throughout the thickness H and the length L and thus gives information of the liquefaction ratio as well as the total liquefied area. As was seen previously, the structure has a significant effect on the liquefaction distribution in the soil deposit. Hence different values of H and L were used to evaluate $Q_{H\cdot L}$. Figure 9 compares the $Q_{H\cdot L}$ values between the models of the B01 and that of the T040 structures for two sets of H and L values : a) H=20m and L=50m, which is the size of the entire finite element model (FEM) and b) H=4m and L=20m, a box under the structure and below the water table level. Note that the results are divided in three groups by liquefaction levels: low (for Q_{FEM} below 0.2), moderate (between 0.2 and 0.5) and high (above 0.5). When the liquefaction index is evaluated throughout FEM, in Figure 9a, results are slightly higher with T040 but in average are fairly similar. This is to be expected since the motions energy is the same and, while under the structure the soil has been modified, other areas will be affected, as was observed in Figure 8a. In general, the differences between the Q_{FEM}results for the two models generally increase for higher Q_{FEM}. However, in average this difference is less than 8%.

In contrast, the Q_{BOX} results shown in Figure 9b differ greatly between the two models. In most cases, the area tested presented higher levels of liquefaction when the T040 structure is used. Note that for the model with B01 structure, several cases present a Q_{BOX} value about 0.2, while for the same cases, Q_{BOX} in the T040 model range between 0.2 to 0.7. On the other hand, in the T040 model, cases that presented Q_{BOX} values about 0.6, can present values ranging from 0.1 to 0.8 in the B01 model. In other words, in the same area, three motions can produce the same level of liquefaction in one model and on the other model, produce either low, moderate or high levels. In order to have a better relation with the motions energy and less influence on the structure used, the liquefaction levels defined by Q_{FEM} will be used in the following section. For further details on this analysis please refer to Montoya-Noguera (2016).

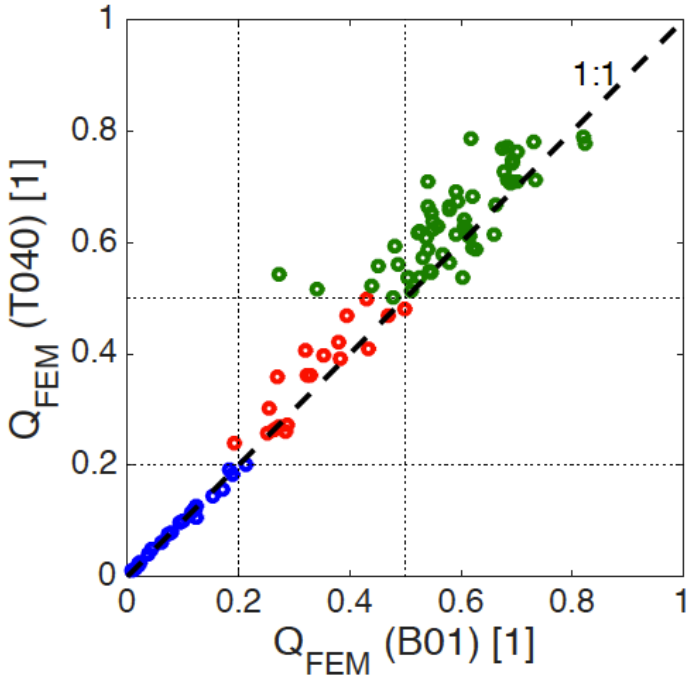

a)

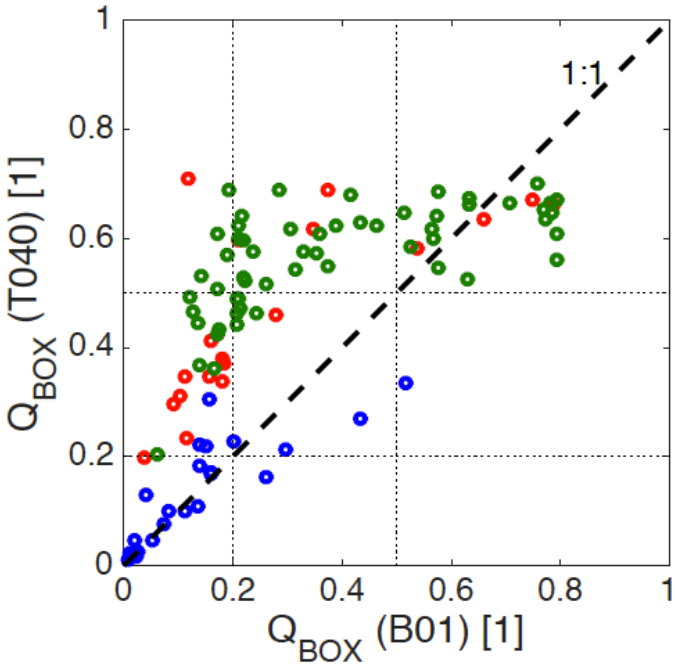

b)

Figure 9: Effect of the structure on the Liquefaction index ($Q_{H\cdot L}$) evaluated at: (a) the entire deposit (Q_{FEM}) and at (b) a box below the structure of size 4x20 (Q_{BOX})

3.1 Effect on the surface acceleration

The amplification (or deamplification) of an earthquake motion due to site effects has been studied for many decades. Some researchers as Trifunac and Brady (1975) and Seed et al. (1976), among others, focused on the correlations between distance from source, earthquake magnitude and site conditions. In engineering practice, site amplification factors are often used to take into account these effects. An example of these factors, is the pioneering work of Idriss (1990) and Dickenson and Seed (1996) based on empirical measurements and engineering judgment of ratios between the peak surface acceleration of a soft deposit (PGA) and the peak horizontal acceleration at outcropping rock (PHA). Advanced numerical models of seismic soil behavior are useful to analyze the nonlinear effects on the ground motion; however if the site is susceptible to liquefaction, when no coupling of Δp_w and soil deformation is present, the model might largely overestimate the peak accelerations at surface.

Concerning the peak ground acceleration (PGA) at the structure's base, Figure 10 shows the comparison between the CPD and DPD values for both structures. For most motions tested the coupling produces a deamplification on the acceleration as it accounts for soil softening due to the pore pressure increase. However, for two motions with T040, where the value of Q_{FEM} is low, the CPD results are greater. These values correspond to high frequency peaks related to the dilatation phase. In general, the differences between the analyses are higher and more dispersive with the B01 structure, specially results for the DPD analysis are doubled for this structure. CPD results of PGA are similar for both structures and appear to be limited by the liquefaction triggering to a maximum value of about 0.25g. The structure weight has an influence on the liquefaction susceptibility but does not seem to affect the PGA value with CPD analysis. In contrast, DPD results of PGA are twice as big with B01 structure which is lighter. As shown in Figure 7a, in the DPD analysis the acceleration at the structure base presents high amplitude spikes at high frequencies which are controlled in the T040 model

because of the structure weight.

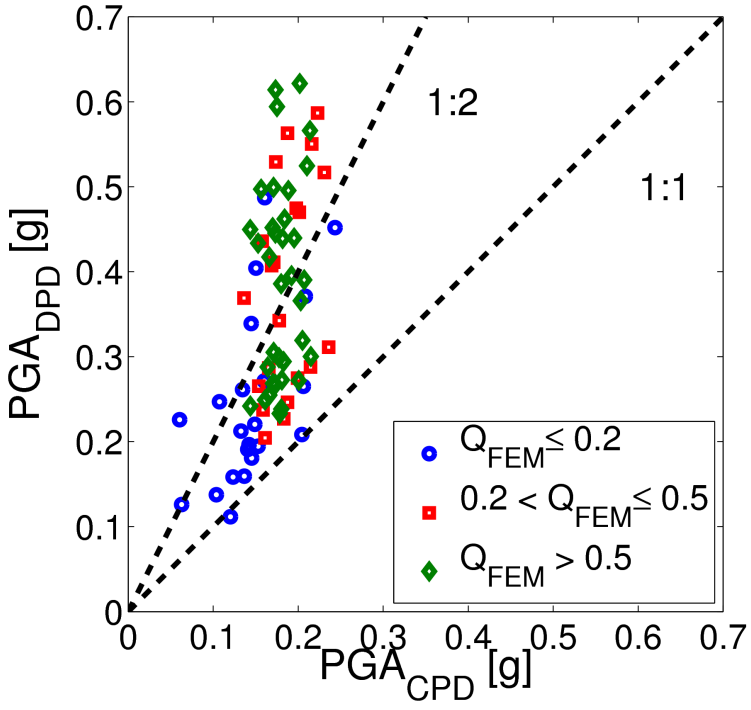

a)

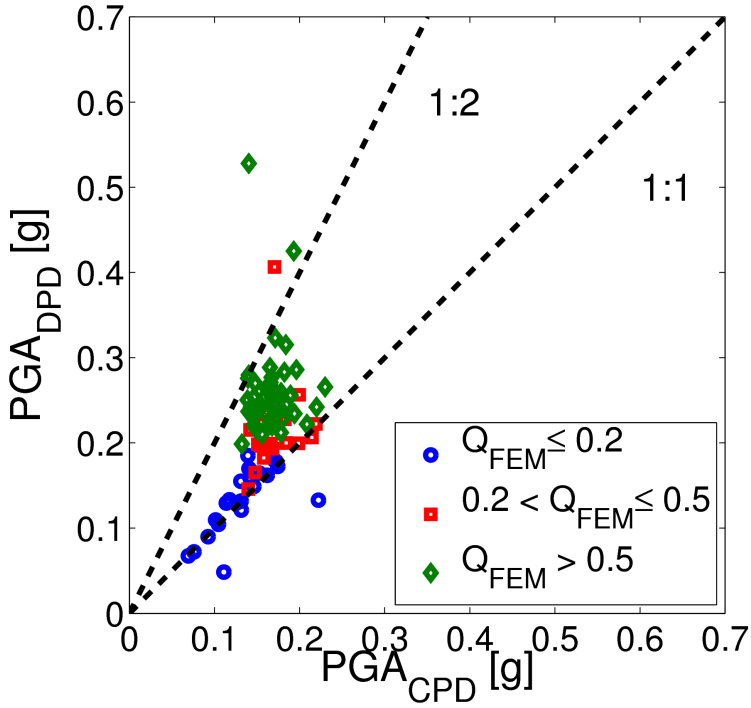

b)

Figure 10: Mean peak ground acceleration (PGA) at structure's base for CPD and DPD analyses for : a) B01 and b) T040 structures

Considering that the structures tested have different predominant periods (T_0), the acceleration response spectra (*PSA*) is evaluated at each T_0 value and the comparison between CPD and DPD is shown in Figure **Error! Reference source not found.**. As the T_0 value of T040 is near the fundamental elastic period of the soil, the behavior presents less dispersion and higher *PSA* values for the decoupled model. On the contrary, with B01 higher dispersion is evidenced specially for the CPD analysis. The combined effect of SSI and

liquefaction is highly variable. With this structure, for almost all cases with low levels of liquefaction and even for some cases with intermediate and high levels, CPD results are higher. Although with the majority of the motions, the results where greater with DPD analysis. Hence, in general, as surface acceleration is concerned, the lack of coupling will produce a conservative analysis.

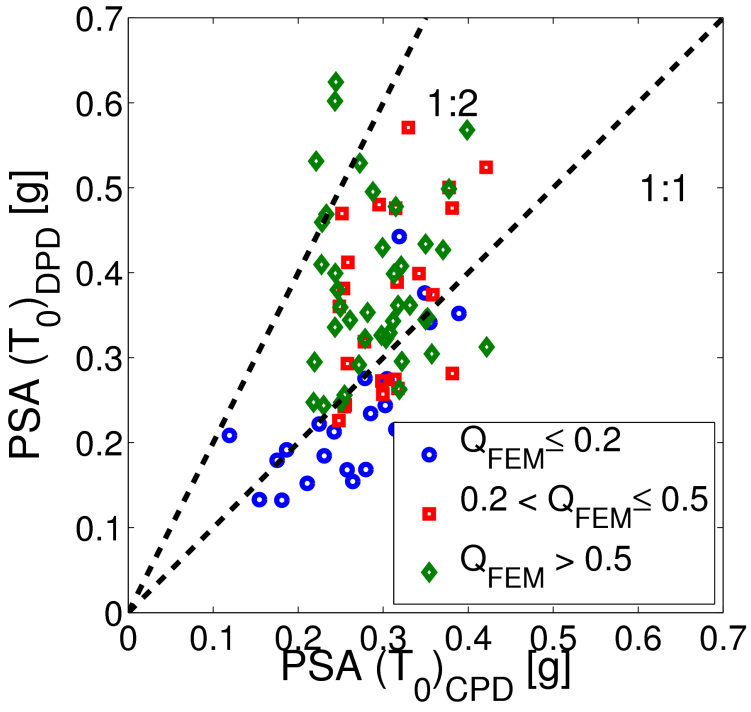

a)

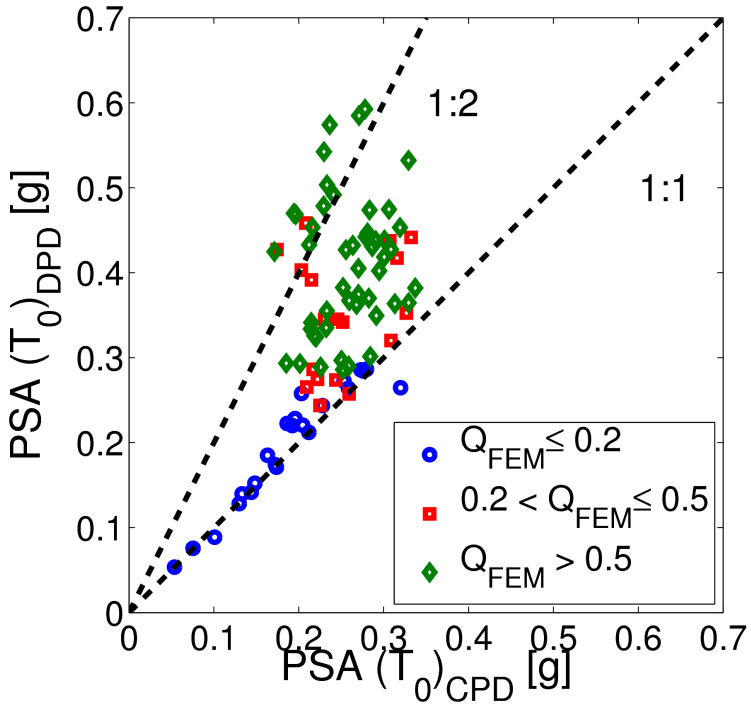

b)

Figure 11: Comparison of CPD and DPD results for the response spectra of acceleration at structure's base evaluated at the predominant structure period: a) B01 and b) T040

3.2 Effect on the structure settlement

In contrast, regarding the relative settlement of the structure with respect to free-field ($|u_z|$),

555 shown in Figure **Error! Reference source not found.**, taking into account the effect of
556 coupling in most cases will result in higher values. This could be prejudicial for the
557 structure's performance. However, as for PSA, some motions presented lower values when
558 CPD is used. Specially for low levels of liquefaction and with the B01 structure. In contract,
559 when liquefaction levels are high and $|u_z|$ is the greatest, the differences between the
560 analyses increase. Note that for some cases, the CPD results are about 10 times greater than
561 the DPD ones.
562
563 As T040 is heavier, $|u_z|$ are more important and with CPD results are above 10cm for
564 approximately half of the motions tested. This value corresponds to the limit for slight
565 damage state of reinforced concrete frame buildings given by Bird et al. (2006). Above it,
566 cracks in structural elements appear and damage has to be repaired. If no coupling was
567 present, this fundamental aspect would be overseen and results will be unconservative or
568 even dangerous for the structure.
569

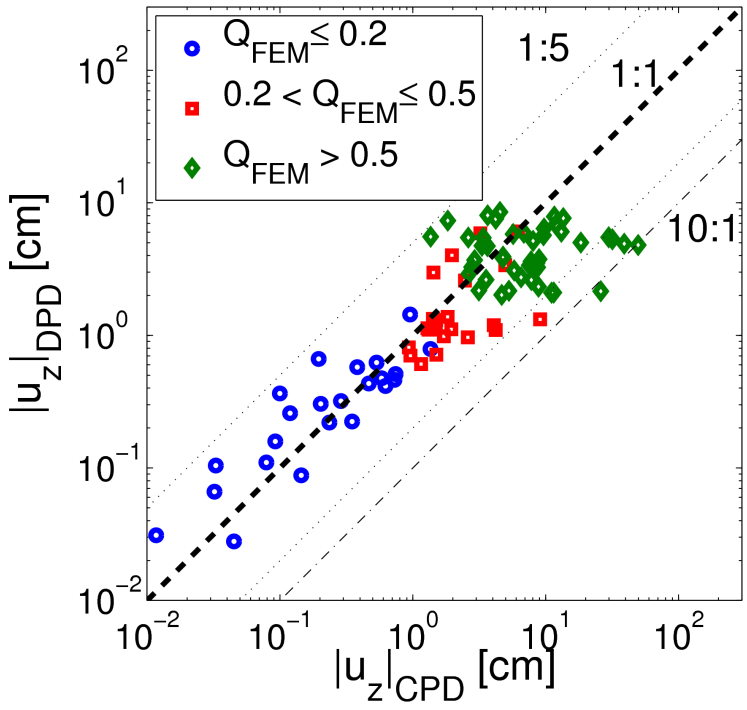

570 a)

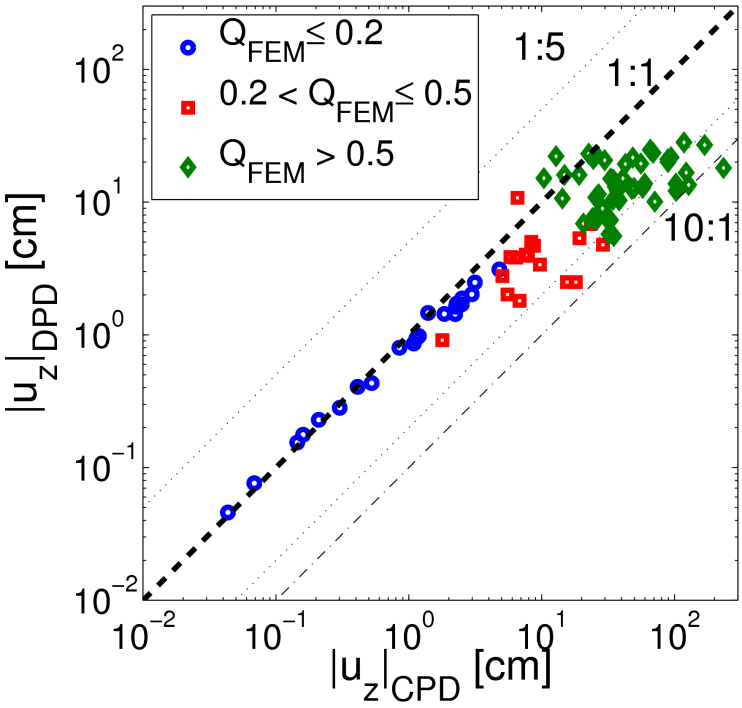

b)

Figure 12: Comparison of CPD and DPD results for the relative settlement with respect to free-field: a) B01 and b) T040

3.3 Effect on the structure seismic demand

Regarding the seismic demand on the structure, the comparison of CPD and DPD results of the maximum inter-story drift (ISD) is shown in Figure **Error! Reference source not found.**. This parameter is appropriate to show the effect on the drift in structures with different height as it normalizes the maximum horizontal displacement evaluated at each level by its corresponding height. It is interesting to note how the two structures present very different results. For B01, the CPD values are greater than the DPD ones for almost all cases; while for T040, it is the contrary.

Recall that the SSI effect for the quasi-elastic behavior is more important for B01, as shown in Figure 4. Hence, with this structure and for low levels of liquefaction the SSI effect is greater than the coupling effect and ISD is higher with CPD analysis. But when the liquefaction level increases, the coupling effect is more important as the soil will attenuate the motion and the structure drift with CPD will be reduced. Concerning T040, the values with the DPD analysis are more than doubled when Q_{FEM} is above 0.5, even four times greater for some cases. Additionally, a high dispersion is evidenced for these values. For models of liquefiable soil where structure nonlinearity is taken into account but there is no coupling of Δp_w with soil deformation, the response could be largely overestimated. This would lead to a conservative design. In contrast, when SSI effects are important, the lack of coupling of Δp_w will lead to an unconservative or prejudicial conception.

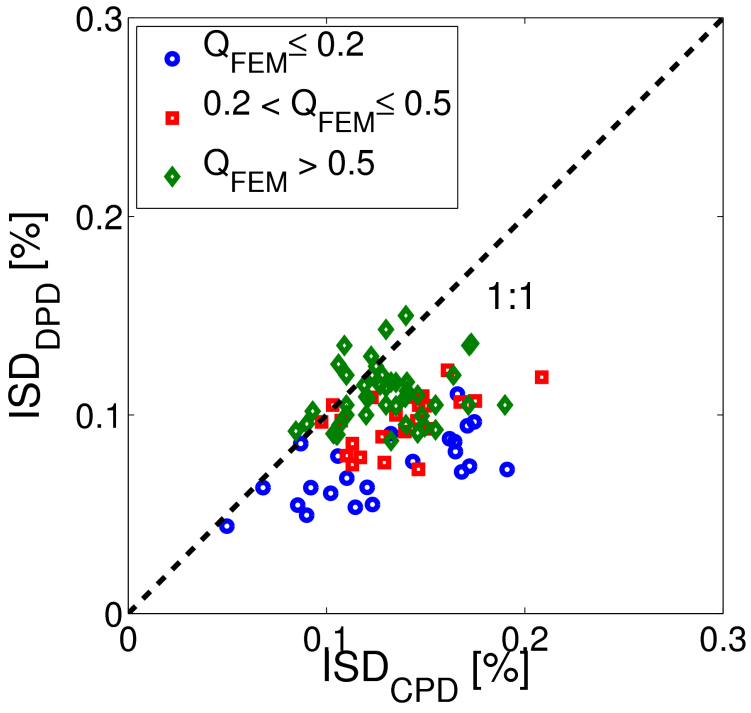

a)

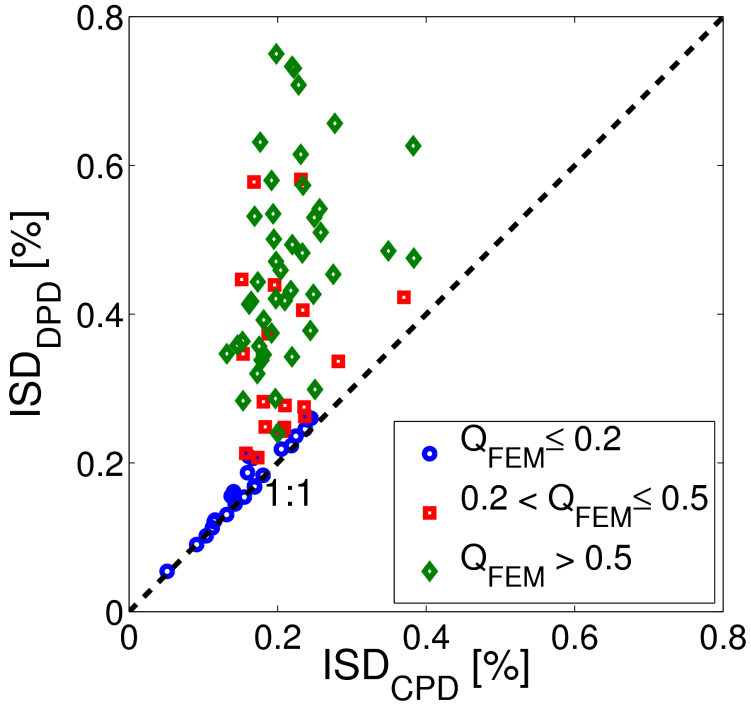

b)

Figure 13: Comparison of CPD and DPD results for the maximum inter story drift: a) B01 and b) T040

Figure 14 shows the nonlinearity evolution of the soil - structure system by analyzing the transfer function ($|TF|$) between the top floor and the free field (FF) for B01. This function takes into account the structure's performance as well as the SSI effects. Results are ranged by the peak horizontal acceleration (PHA) recorded at the outcropping rock. Additionally, the fundamental elastic frequency of the soil deposit (f_0) and that of the structure in fixed base condition (f_{str}^{FB}) are shown as reference. With DPD analysis, a lower amplitude of the predominant frequency even for low PHA values. This deamplification drops drastically after about 0.7g and the frequency is reduced by more than 1Hz for the highest PHA. In contrast,

609 with CPD analysis the deamplification is smaller and almost no frequency shift is evidenced.
610 This can be explained by the liquefaction presented in the deposit that can isolate the SSI
611 effect between the surficial soil and the structure.
612

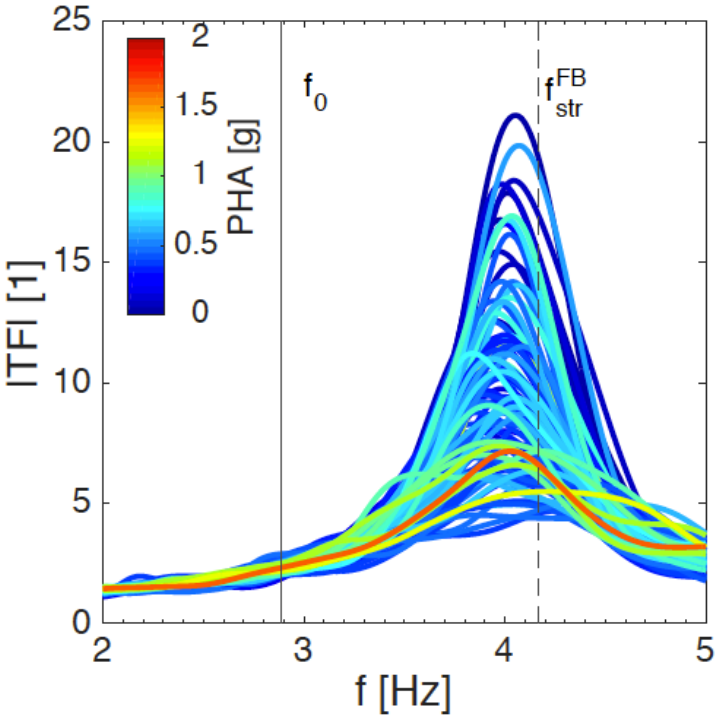

613 a)

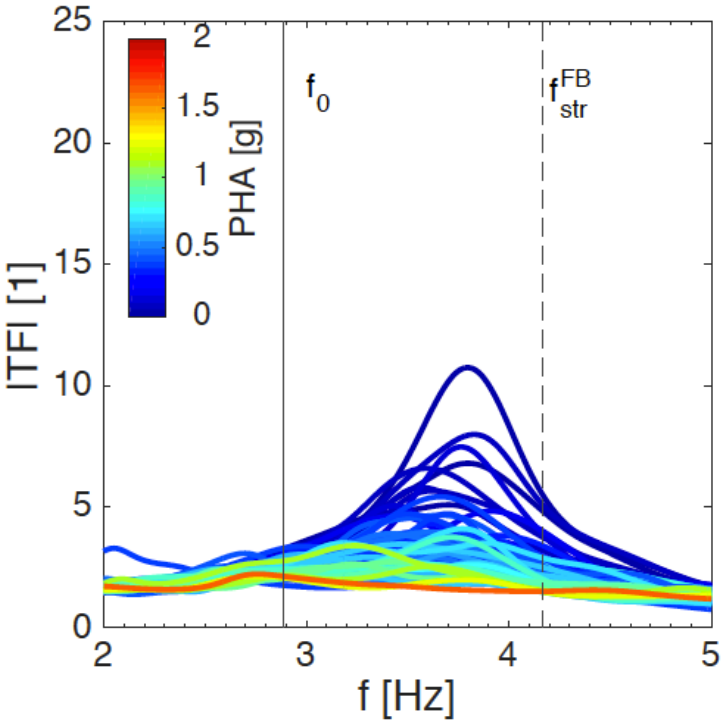

614 b)

615 Figure 14: Nonlinearity evolution at the structure's |*TF*| (Top/FF) for B01 with a) CPD and b)
616 DPD analyses
617
618 3.4 Comparison with 1D models
619 Finally the effect of pore pressure generation on the surface acceleration is compared
620 between a 1D FF model and the 2D soil-structure model. When no soil-structure interaction

(SSI) is present, the wave propagation is evaluated on a soil column and the altered spectra of acceleration is used on the structure's model. In Figure 15 the response spectra ratio (RSR) evaluated at the surface of a 1D model is compared to that of the base of each structure. In this figure the effects of both the SSI and the coupling of Δp_w and soil deformation can be analyzed. RSR is defined by:

$$RSR(T) = PSA_{CPD}(T)/PSA_{DPD}(T) \quad (5)$$

The mean values for each liquefaction index level are shown in Figure 15. The results for the 1D model are shown in dashed lines and are the same in both figures, as no structure is present. However, the results with the structures vary greatly. It seems that the SSI effect is important for B01 while it is almost negligible for T040 - as 1D and 2D results are roughly similar. Specially, at the structure's predominant period, RSR is affected for B01 (T_0=0.24s) where with low liquefaction levels the CPD amplification is even 25% higher than the DPD one; while for T040 no change is visible at this period (T_0=0.4s). Differences between 1D and 2D results are greater for short periods, below 0.2s and more important for B01. Which means that the coupling effects are greater when SSI effects are more important. However, even if RSR appears to be related to the liquefaction level, the mean values for high and intermediate levels are similar in all the period range used and specially for B01 results. This aspect is worth mentioning as it means that although liquefaction is not triggered, the pore pressure migration due to the structure's effect on the soil modifies the acceleration response at the structure's base. Hence, a CPD analysis is preferred when modeling 2D SSI even if liquefaction potential is low.

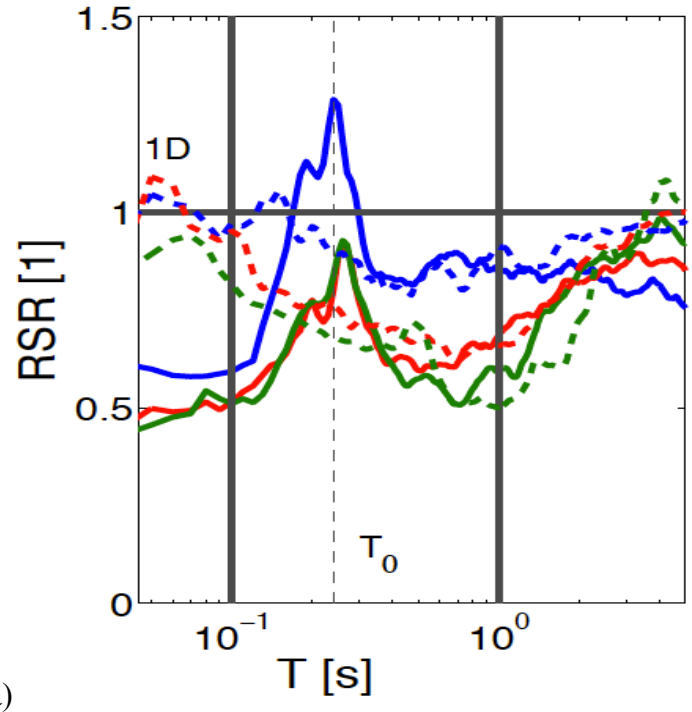

a)

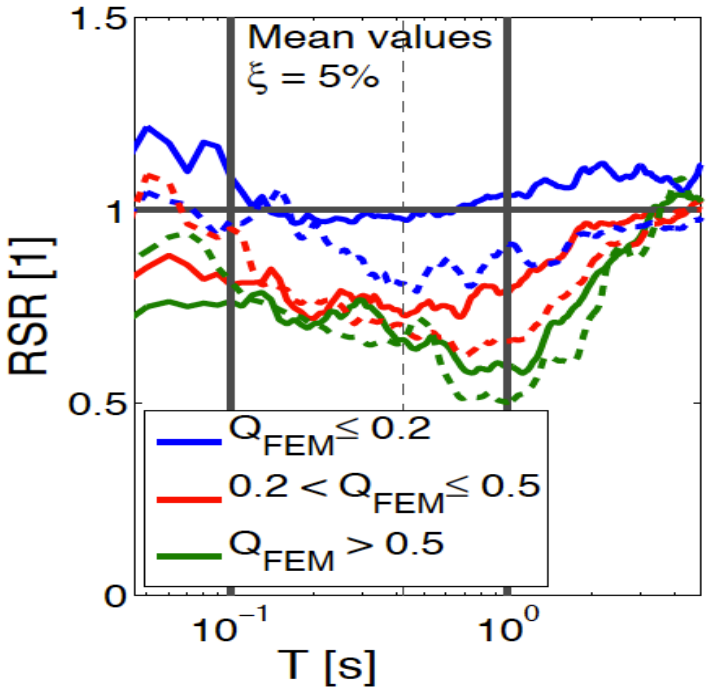

b)

Figure 15: RSR at 1D model and at structure's base for: a) B01 and b) T040

4 CONCLUSIONS

A finite element analysis was used to investigate the effect of coupling excess pore pressure and soil deformation on a soil-structure model. Two mechanically-equivalent analyses were performed with 90 unscaled earthquake motions: one taking into account coupling (CPD) and one fully-drained (DPD). The same effective-stress model was used for the calculations and the initial elastic behavior was proved to be the same. The present study aimed to highlight the importance of accurately model liquefiable soils in order to improve performance-based earthquake engineering (PBEE). One of the main findings of this study is that when models are fully drained, less shear strains are developed hence the relative settlement of the structure is underestimated for most motions and both structures tested. Even if in free-field (FF), DPD analysis presented higher settlement, the structure's weight affects the soil behavior and hence the structure's settlement with respect to FF is in general underestimated with DPD models. Additionally, if the SSI effects are significant, i.e. when the predominant period of the structure is near to that of the soil, the maximum ISD is consistently underestimated by the DPD analysis. In this regard, the use of DPD models will not be recommended for a PBEE design. Two main effects are involved in this analysis: the coupling of excess pore pressure and soil deformation and the interactions between the soil deposit and the structure. These can be beneficial or detrimental for different EDPs but the analysis should include both as it seems that the complex relation between them will vary for each motion, soil and structure tested.

The relation of both SSI and CPD effects was shown to be highly complex. Thus, the effects of CPD could be further evaluated for other soil deposits and other structures in order to increase the reliability of the results. In addition to the nonlinearity of the soil, the structure's nonlinearity could be further enriched comprehending the evaluation of damage and failure. The present study focused on the comparison between drained and coupled analyses, however, it would be interesting to also compare the response of perfectly undrained analysis available on several commercial softwares and performed by practitioners. More on this topic will be analyzed in a future work Furthermore, some challenges are still to be acknowledged.

Comparisons of CPD and DPD models with vertical array data in liquefiable soils could be helpful to better understand the importance of coupling excess pore pressure and deformations. Additionally, physical modeling of structures founded on liquefiable soil could be performed in shaking tables and centrifuge tests to further validate the relation between both SSI and CPD effects.

5 ACKNOWLEDGMENT

The work described in this paper was partly supported by the SEISM Paris Saclay Research Institute. This support is gratefully acknowledged.

References

V.P. Drenevich and F.E. Richart. Dynamic prestraining of dry sand. *Soil Mechanics and Foundations Division*, 96 (SM2):453–469, March 1970. PROC PAPER 7160.

R. Dobry and W.F. Swiger. Threshold strain and cyclic behavior of cohesionless soils. In *3rd ASCE/EMDE Specialty Conference*, pages 521–525, Austin, Texas, September 1979.

R. Dobry, R.S. Ladd, F.Y. Yokel, R.M. Chung, and D. Powell. Prediction of pore water pressure buildup and liquefaction of sands during earthquakes by the cyclic strain method. *NBS Building Science Series 138*, page 150, 1982.

N. Yoshida and S. Iai. Nonlinear site response and its evaluation and prediction. In *2nd International Symposium on the Effect of Surface Geology on Seismic Motion*, pages 71–90, Yokosuka, Japan, 1998.

A. Hartvigsen. Influence of pore pressures in liquefiable soils on elastic response spectra. Master's thesis, University of Washington, Seattle, 2007.

N. Yoshida. Applicability of total stress seismic ground response analysis under large earthquakes. In *COMPDYN2013: 4th ECCOMAS Thematic Conference on Computational methods in structural Dynamics and earthquake engineering*, page 13, Kos Island, Greece, June 2013.

S. Montoya-Noguera and F. Lopez-Caballero. Effect of coupling excess pore pressure and deformation on nonlinear seismic soil response. *Acta Geotechnica*, 11(1):191–207, February 2016. 10.1007/s11440-014-0355-7.

S.L. Kramer, A.J. Hartvigsen, S.S. Sideras, and P.T. Ozener. Site response modeling in liquefiable soil deposits. In *4th IASPEI / IAEE International Symposium: Effects of Surface Geology on Seismic Motion*, page 13, University of California Santa Barbara, august 2011.

H.B. Seed and I.M. Idriss. Simplified procedure for evaluating soil liquefaction potential. *Journal of the Soil Mechanics and Foundations Division*, 107(SM9):1249–1274, 1971.

I.A. Beresnev and K.L. Wen. Nonlinear site response: a reality? *Bulletin of the Seismological Society of America*, 86 (6):1964–1978, 1996.

J.R. Gingery, A. Elgamal, and J.D. Bray. Response Spectra at Liquefaction Sites during Shallow Crustal Earthquakes. *Earthquake Spectra*, 2014. 10.1193/101813EQS272M. In press.

B.S. Chiou and R.R. Youngs. An NGA model for the average horizontal component of peak ground motion and response spectra. *Earthquake Spectra*, 24(1):173–215, 2008.

D. Aubry and A. Modaressi. *GEFDyn - manuel scientifique*. Ecole Centrale Paris, France: LMSSMat, July 1996.

E. Saez, F. Lopez-Caballero, and A. Modaressi-Farahmand-Razavi. Inelastic dynamic soil-structure interaction effects on moment-resisting frame buildings. *Engineering structures*, 51(1):166–177, 2013. 10.1016/j.engstruct.2013.01.020.

E. Foerster and H. Modaressi. A diagonal consistent mass matrix for earthquake site response simulations. In *4th International Conference on Earthquake Geotechnical Engineering (ICEGE)*, Thessaloniki, Greece, June 2007a. Paper: 1242.

O.C. Zienkiewicz and T. Shiomi. Dynamic behavior of saturated porous media: the generalised biot formulation and its numerical solution. *International Journal for Numerical and Analytical Methods in Geomechanics*, 8(1):71–96, 1984.

O.C. Zienkiewicz and R.L. Taylor. *The Finite element method, solid and fluid mechanics, dynamics and non-linearity*, volume 2. McGraw-Hill Book Company, London, 4th edition, 1991.

H. Modaressi. *Modélisation numérique de la propagation des ondes dans les milieux poreux anélastiques*. PhD thesis, Laboratoire MSSMat, Ecole Centrale Paris, Châtenay-Malabry, France, 1987. Advisor: Denis Aubry.

K. Terzaghi. *Theoretical Soil Mechanics*. John Wiley & Sons, 1943.

F. Lopez-Caballero and A. Modaressi. Numerical analysis: Specification and validation of used numerical methods. FP7-SME-2010-1-262161, PREMISERI project, Paris, France, 2011.

H. Modaressi and I. Benzenati. Paraxial approximation for poroelastic media. *Soil Dynamics and Earthquake Engineering*, 13 (2):117–129, 1994.

D. Aubry, D. Chouvet, A. Modaressi, and H. Modaressi. GEFDyn 5, logiciel d'analyse du comportement statique et dynamique des sols par elements finis avec prise en compte du couplage sol-eau-air, 1985.

E. Foerster and H. Modaressi. Nonlinear numerical methods for earthquake site response analysis II- case studies. *Bulletin of Earthquake Engineering*, 5(3): 325–345, 2007b. 10.1007/s10518-007-9034-5.

J. Régnier, L. F. Bonilla, P. Y. Bard, D. Assimaki, Y. Hashash, and et al. International benchmark on numerical simulations for 1D, non-linear site response (PRENOLIN): verification phase based on canonical cases. *Bulletin of the Seismological Society of America*, 2015. In review.

S. Sica, L. Pagano, and A. Modaressi. Influence of past loading history on the seismic response of earth dams. *Computers and Geotechnics*, 35(1):61–85, 2008. 10.1016/j.compgeo.2007.03.004.

L.A. Berenguer Todo-Bom. *Numerical modeling of soil-pile interaction considering grain breakage in finite deformations*. PhD thesis, Ecole Centrale Paris, Paris, France, 2014.

D. Aubry, J.C. Hujeux, F. Lassoudiere, and Y. Meimon. A double memory model with multiple mechanisms for cyclic soil behavior. In *International Symposium on Numerical Modeling in Geomechanics*, pages 3–13, Balkema, 1982.

J.C. Hujeux. Une loi de comportement pour le chargement cyclique des sols. In *Génie Parasismique*, pages 278–302, France, 1985. Presses ENPC. Edited by V. Davidovici.

F. Lopez-Caballero and A. Modaressi-Farahmand-Razavi. Assessment of variability and uncertainties effects on the seimic response of a liquefiable soil profile. *Soil Dynamics and Earthquake Engineering*, 30 (7):600–613, 2010.

766 F. Lopez-Caballero, A. Modaressi-Farahmand-Razavi, and H. Modaressi. Nonlinear
767 numerical method for earthquake site response analysis i — elastoplastic cyclic model and
768 parameter identification strategy. *Bulletin of Earthquake Engineering*, 5(3): 303–323, jun
769 2007. 10.1007/s10518-007-9032-7.

770 V. Prakash, G. Powel, and S. Campbell. *DRAIN-2DX Base program description and user*
771 *guide: version 1.10*. Dept. of Civil Engineering, University of California, Berkeley, 1993.
772 UCB/SEMM-1993/17.

773 F.J. Vechio and M.B. Emara. Shear deformation in reinforced concrete frames. *ACI*
774 *Structural journal*, 89(1):46–56, 1992.

775 HAZUS-MH MR3. *Multi-hazard Loss Estimation Methodology*. Federal Emergency
776 Management Agency, Washington, DC, 2003.

777 G. Mylonakis and G. Gazetas. Seismic soil–structure interaction : beneficial or detrimental?
778 *Journal of Earthquake Engineering*, 4(3): 277–301, jul 2000. 10.1080/13632460009350372.

779 S. Koutsourelakis, J.H. Prévost, and G. Deodatis. Risk assessment of an interacting structure-
780 soil system due to liquefaction. *Earthquake Engineering and Structural Dynamics*, 31
781 (4):851–879, 2002. 10.1002/eqe.125.

782 R. Popescu, J. H. Prévost, G. Deodatis, and P. Chakrabortty. Dynamics of nonlinear porous
783 media with applications to soil liquefaction. *Soil dynamics and earthquake engineering*, 26
784 (6):648–665, 2006.

785 M.D. Trifunac and A.G. Brady. A study on the duration of strong earthquake ground motion.
786 *Bulletin of the Seismological Society of America*, 65(3):581–626, 1975.

787 H.B. Seed, J. Murarka, J. Lysmer, and I.M. Idriss. Relationships between maximum
788 acceleration, maximum velocity, distance from source and local site conditions for
789 moderately strong earthquakes. *Bulletin Seismological Society of America*, 66 (4):1323–1342,
790 1976.

791 I.M. Idriss. Influence of local site conditions on earthquake ground motions. In *Proc. of IV*
792 *U.S. Nat. Conf. on Earthquake Engineering*, volume 1, pages 55–57, Palm Springs,
793 California, 1990.

794 S.E. Dickenson and R.B. Seed. Nonlinear dynamic response of soft and deep cohesive soil
795 deposits. In *Proceedings of the international workshop on site response subjected to strong*
796 *earthquake motions*, volume 2, pages 67–81, Yokosuka, Japan, 1996.

797 M. Shinozuka and K. Ohtomo. Spatial severity of liquefaction. In *Proceedings of the second*
798 *US-Japan workshop in liquefaction, large ground deformation and their effects on lifelines*,
799 pages 193–206, New York, 1989. NCEER.

800 S. Montoya-Noguera. *Assessment and mitigation of liquefaction seismic risk: Numerical*
801 *modeling of their effects on SSI*. PhD thesis, CentraleSupélec, Paris-Saclay University,
802 Châtenay-Malabry, France, 2016.

803 J.F. Bird, J.J. Bommer, H. Crowley, and R. Pinho. Modelling liquefaction-induced building
804 damage in earthquake loss estimation. *Soil Dynamics and Earthquake Engineering*, 26
805 (1):15–30, 2006. 10.1016/j.soildyn.2005.10.002.